Longitudinal Analysis of Steel-Concrete Composite Box Girder Decks

Comparison between the Classical Formulations and the Generalized Beam Theory

Luís João Ferreira Vieira

Abstract

Asymmetrical loads on box girder bridge decks produce not only bending but also torsion with warping and distortion of the cross-section. The latter two may prove to be relevant for the longitudinal analysis and design of the box girder but their effects are difficult to assess using shell finite element models. Two alternative bar-type analysis methods are presented that preserve the structural significance of each main type of cross-section deformation "mode": the first covers the classical prismatic bar theories of bending and torsion with warping, the beam on elastic foundation analogy for the analysis of distortion, also known as "folded plate action", and a simplified semi-empirical methodology for the consideration of shear lag effects. The second refers to a finite element method based on the Generalized Beam Theory, which is geared towards the longitudinal analysis of homogenous/composite thin-walled prismatic bars including arbitrary in-plane and out-of-plane (warping) deformation. Comparisons are established between the two latter methods, in terms of theoretical background and numerical results, using two case studies. Within the analysis of the numerical examples, the influence of intermediate diaphragms in the longitudinal behaviour is investigated, referring particularly to the participation of torsion and distortion deformation modes. Some insightful notes are given concerning the design effects of intermediate diaphragms and the governing load configurations for box girder design.

1. Introduction

In light of the modern-day economical demands, designers have progressively searched to reduce the overall weight and thickness of the concrete walls and steel plates in box girder bridge decks, leading almost unavoidably to very slender and deformable cross-sections (Pedro, 1995). As a direct consequence, the effects of cross-section out-of-plane (warping) and in-plane (distortion) deformation have become more relevant and can turn out to be very important in the design verifications of composite box girders.

The study of torsion and distortion in composite box girder decks is therefore an important issue from a practical standpoint, but also a relatively complex one, which is why it is usually solved resorting to shell finite element models that do not allow a clear identification of the different structural effects and also generate a huge amount of data that must be post-processed by the designer.

The present work is developed around two alternative methods that maintain the structural significance of bending, torsion, distortion and shear lag, and may be used in the evaluation of the longitudinal stresses. The first relates to the classical approaches to obtain the longitudinal equilibrium equations and is henceforth designated as the "Classical Formulations". It encompasses the Euler Beam theory for bending, the warping torsion theory presented by Benscoter (1954) and the folded plate theory based on a beam on elastic foundation analogy first introduced by Wright, Abdel-Samed, & Robinson (1968) as a way of accounting for distortion in box girders. It also contains the simplified method for the determination of the non-linear stress distribution brought by shear lag effect in bending as presented in B.S.I. (2004). The second method involves the use of the Generalized Beam Theory (GBT), a recently emerging formulation for thin-walled prismatic members which has shown very promising results, including for box-girder bridges (Gonçalves & Camotim, 2010), but is still generally unknown to designers. In this theory, it is considered that the overall response of the beam-type structure is described by the superposition of pre-defined cross-section deformation modes (including bending, torsion, distortion and other modes), whose amplitudes along the longitudinal axis constitute the problem unknowns .

This work sheds some light into these two methods used to perform the longitudinal analysis of box girder decks, in terms of their formulations and, most especially, of the results they provide both in terms of total longitudinal normal stresses and in terms of the participation of bending, torsion, distortion and shear lag. There is a specific focus in the analysis of steel-concrete composite box girders with intermediate diaphragms, whose relevance in reducing the torsional and distortional stresses is well-known but not simple to assess.

Reference is made to straight, thin-walled, unicellular box girders which behave elastically and are symmetric about the vertical axis. For the particular case of steel-concrete composite bridges, they are assumed to be composed of a reinforced concrete upper plate or deck, two steel web plates and one bottom plate, also made of steel. In the analysis, the upper flange will be taken approximately as a non-cracked and non-reinforced slab, and the shear connection slip is disregarded.

2. Overview of Classical Formulations

The longitudinal analysis of box girders can be performed according to the Classical Formulations for bending, torsion and distortion. According to the work by Pedro (1995), based on the IABSE publication by Schlaich & Scheef (1982), the analysis procedure for a thin-walled box girder subjected to a generic vertical loading, such as the one presented in Figure 1, can be obtained by superposition of the results from the following sub-analyses:

1) Longitudinal analysis of the beam assuming a rigid cross-section. Vertical and torsional loadings derive from direct integration along the transverse direction. Torsional and bending moment diagrams are obtained, as well as the longitudinal stresses in the cross-section due to bending. If shear lag effects are to be considered, the modified bending stress distribution is obtained using effective widths.

2) Transverse analysis:

2.1) Analysis of the top flange considering it to be rigidly fixed at the webs – see Figure 1a1. Vertical loads are henceforth replaced by equivalent forces and moments, applied at the top of the webs. In this work, it was assumed that vertical loads eccentric with respect to the webs are carried directly to the nearest point of the web plate, i.e., no in-plane load degradation is considered.

2.2) Analysis of a transverse strip of longitudinal length $\Delta x = 1$ as a frame subjected to eccentric forces (m_A, p_A), (m_B, p_B) – Figure 1a2:

2.2.1) Division of the applied loads into symmetric (Figure 1b1) and anti-symmetric (Figure 1b2) parts

2.2.2) Calculation of the cross-section symmetric transverse bending. For symmetrical loading, the distribution of the transverse bending moments is hereby obtained by adding these results to those derived in 2.1). The effect of rigid body displacement of the cross-section due to longitudinal bending is already addressed in 1)

2.2.3) Division of the anti-symmetrical part into torsional and distortional subsystems. The effect of bi-shear in the determination of the distortional loads is commonly neglected because the error involved in this assumption is usually small (Fan & Helwig, 2002) and brings significant gains in terms of simplicity. Therefore, the torsional response can be given by pure torsional loads that are obtained directly through integration of the shear flow given by Bredt's formula.

$$p_{w,PureT} = \left(\frac{b_w}{(b_t + b_b)d}\right)(p_{anti} b_t + 2m_{anti}),$$
$$p_{t,PureT} = \left(\frac{b_t}{b_w}\right) p_{w,PureT}, \qquad (1)$$
$$p_{b,PureT} = \left(\frac{b_b}{b_w}\right) p_{w,PureT}.$$

The distortional loads for the anti-symmetrical vertical loads can be obtained knowing that (i) the sum of the vertical components of $p_{w,PureT}$ and $p_{w,d}$ and (ii) the distortional system is self-equilibrated. For the anti-symmetrical nodal moments, the distortional loads are obtained considering the transverse frame behaviour (Schlaich & Scheef; 1982).

$$p_{w,d} = \left(\frac{b_b\, b_w}{(b_t + b_b)d}\right) p_{anti} b_t - \left(\frac{2b_w}{b_b d}\right)\left(\frac{\beta}{1+\beta} + \frac{r_t - 3\beta - 2\beta r_b}{(r_t + 2)(r_b + 2) - 1}\right) m_{anti},$$
$$p_{t,d} = \left(\frac{b_b}{b_w}\right) p_{w,d}, \qquad (2)$$
$$p_{b,d} = \left(\frac{b_t}{b_w}\right) p_{w,d}.$$

2.2.4) Finally, the effects of the distortional subsystem can be accounted for through a theoretical model of a beam supported on elastic springs that is intended to replicate the effect of cross-section distortion throughout the span. This analogy was originally proposed by Wright, Abdel-Samed, & Robinson (1968). Analysing the web as a beam on an elastic foundation, one can obtain distortional warping stresses to be added up to the ones provoked by bending and torsional warping.

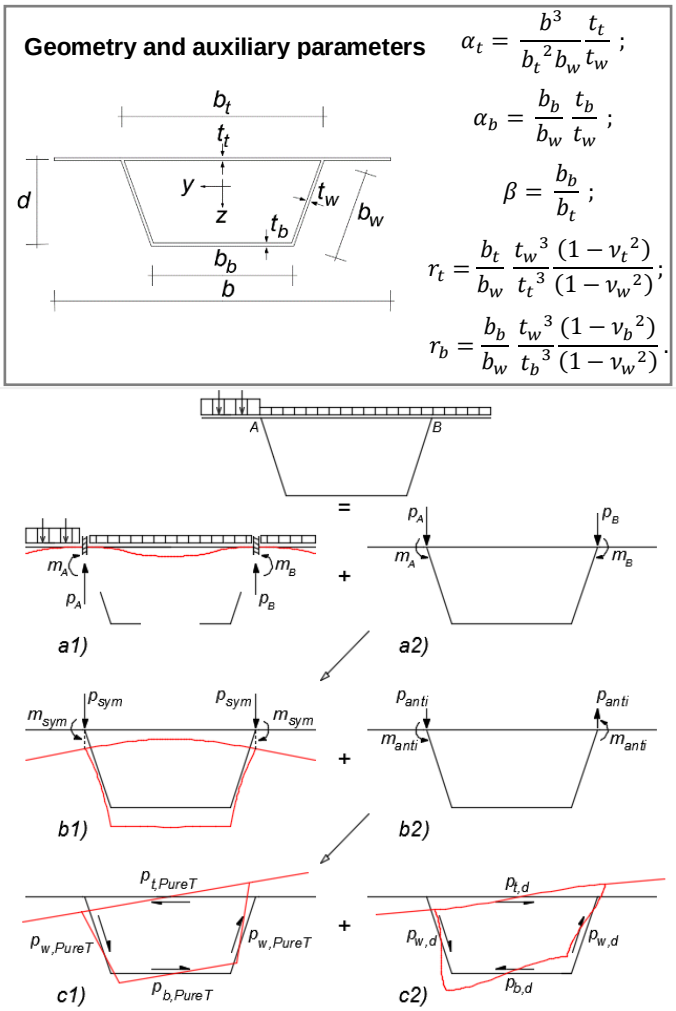

Figure 1 – Load subdivision in Classical Formulations

2.1. Elastic Bending

The longitudinal bending stresses can be determined according to the Euler-Bernoulli Beam theory. This formulation considers that plane sections remain plane and normal to the axis (Bernoulli's Hypothesis) and that sections are free to deform in their own plane, i.e. $\sigma_{yy} = \sigma_{zz} = \tau_{yz} = 0$ (Navier's Hypothesis).

When dealing with composite steel-concrete box girders it is necessary to determine an equivalent homogenized cross-section, in which the reference material is usually steel (the reinforced concrete slab is replaced by an equivalent steel plate with a thickness equal to ${t_t}^S = t_t\, E_c/E_s = t_t\, /n$).

The longitudinal equilibrium equation for bending reads

$$\frac{d^4 v}{dx^4} EI_y = p(x), \qquad (3)$$

where v is the vertical displacement of the beam, E is Young's modulus, I_y is the minor axis moment of inertia and p is the vertical load.

The longitudinal normal stresses in steel $(\sigma_{xx})_b^S$ can be obtained as a function of bending moment M_y and of the vertical coordinate with respect to the centre of gravity z through

$$\sigma_b = \frac{M_y}{I_y} z. \qquad (4)$$

The stresses in the reinforced concrete components can be retrieved by using

$$\sigma_b^C = \frac{\sigma_b^S}{n}. \qquad (5)$$

2.2. Shear Lag Effect

The elastic bending theory just presented neglects the shear deformability of the cross-section. However, in wide flanges, this deformability can lead to a significant change in the longitudinal stresses with respect to the ones obtained from Euler-Bernoulli beam theory (Chen & Yen, 1980). Due to the so-called shear lag effect, the stresses increase in regions close to web-flange junctions and decrease with the distance to these junctions.

Although some analytical solutions can be found (see for example Chen & Yen (1980)), they are usually replaced by a more practical and common way of accounting for this effect, which consists in making use of a cross-section with effective (reduced) widths for the wide flanges (see Figure 2). More than one definition can be used for evaluating these parameters. In this work, reference is made to the approach followed in B.S.I. (2004), which is related to the stress distribution. Here, the effective width is considered to be the width that sustains a force equal to that in the actual flange, assuming the longitudinal stresses to be at the same time constant and equal to the maximum longitudinal stress of the non-linear stress distribution (Castro, Elghazouli, & Izzuddin, 2007).

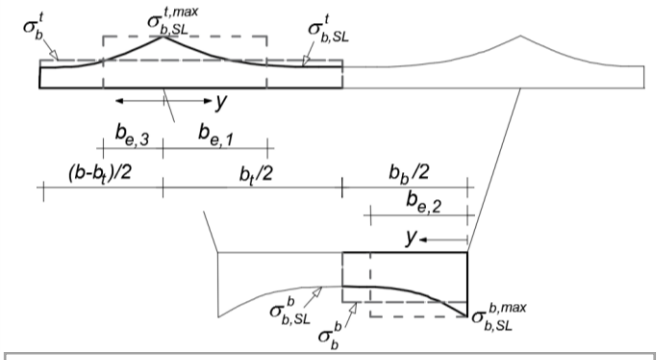

$$b_{e,1} = \Psi_1 b_t/2 \;;\; b_{e,2} = \Psi_2 b_b/2 \;;\; b_{e,3} = k\,\Psi_3 (b - b_t)/2$$
$$k = 1 - 0.15\,(b - b_t)/2l$$

Figure 2 – Non-linear distribution of the longitudinal bending stresses in top and bottom flanges

The maximum longitudinal stresses at the top and bottom flange-web intersections can be retrieved by taking advantage of the results from standard Euler-Bernoulli beam theory:

$$\sigma_{b,SL}^{t,max} = \sigma_b^t \frac{b}{2\left(b_{e,1} + b_{e,3}\right)}, \quad \sigma_{b,SL}^{b,max} = \sigma_b^b \frac{b_b}{2b_{e,2}}. \qquad (6)$$

Finally, the transverse non-linear stress distribution of the whole cross-section may be approximately calculated through the quartic expressions presented in B.S.I. (2004).

Even though the normal stress distribution is non-linear, the shear lag phenomenon itself nonetheless manifests itself in linear elastic problems and depends directly on the shear modulus G. For this reason, and assuming that the ratio between the concrete and steel shear moduli is approximately equal to the ratio between the corresponding Young's moduli (assumed uncracked concrete), (5) can still be employed:

$$\left(\frac{t_t}{t_t{}^S}\right)_{b,SL} = \frac{E_s}{E_c}\frac{1+\upsilon_c}{1+\upsilon_s} = \frac{E_s}{E_c}\frac{1+0.2}{1+0.3} \approx \frac{E_s}{E_c} = \left(\frac{t_t}{t_t{}^S}\right)_b = n. \qquad (7)$$

2.3. Torsion

In each cross-section, the torsional moment T is equilibrated by the sum of two twist resisting effects: the uniform or Saint-Venant torsion (T_{SV}), which is essentially characterized by a constant circulatory shear flow in the cross-section, and the non-uniform or warping torsion (T_w), which is related with the development of bi-moment and bi-shear stresses (Kollbrunner & Basler, 1969).

2.3.1. Uniform Torsion

In closed thin-walled cross-sections, such as the case of common box girder bridges, the torsional stiffness is almost entirely given by a uniform shear flow (q_{SV}) circulating around the closed-contour (the linear through-thickness component of the shear stresses may be neglected (Kollbrunner & Basler, 1969)). This shear flow is given by Bredt's formula:

$$q_{SV} = \frac{T_{SV}}{2\,A_0} = \frac{T_{SV}}{(b_b + b_t)\,d}. \qquad (8)$$

The shear flow can be related to the rate of twist as follows

$$\phi_{,x} = \frac{T_{SV}}{G\,J}, \qquad (9)$$

$$J = \frac{4\,{A_0}^2}{\oint \frac{ds}{t}}, \qquad (10)$$

being J the Saint Venant torsional constant for unicellular box girders and A_0 the area enclosed by the mid-section walls.

It is also possible to define the shape of the warping displacements u as a function of the rate of twist and of a normalized unit warping function $\widetilde{u_S}(s)$, with respect to the shear centre:

$$u(s) = -\phi_{,x}\,\widetilde{u_S}(s), \qquad (11)$$

$$\widetilde{u_S}(s) = \int_0^s r\,ds - \frac{2\,A_0}{\oint \frac{ds}{t}} \int_0^s \frac{ds}{t}. \qquad (12)$$

The detailed process for the determination of $\widetilde{u_S}(s)$ may be found in Kollbrunner & Basler (1969) or in Pedro (1995).

2.3.2. Warping Torsion

In common box-girder bridges subjected to torsion there is a natural tendency for warping of the cross-section. When the warping displacement is constrained, a set of torsional warping stresses σ_w is generated, along with corresponding shear stresses τ_w to be added to those related to uniform torsion, τ_{SV}. The interaction between the these stresses and those obtained by Saint-Venant theory alter the displacements on a closed cross-section, making (11) invalid, since $\phi(x)$ is strictly dependant on Saint-Venant shear flow q_{SV}. For this reason, it is necessary to consider a new auxiliary function $\chi(x)$, to be dependent on the total shear flow $q = q_{SV} + q_w$. As a result, it is assumed that

$$u(x,s) = -\tilde{u}_S(s)\frac{d\chi}{dx}\,, \qquad (13)$$

where χ is a function to be evaluated by taking its derivative as an analogy for the twist angle of the cross section employed for uniform torsion.

The stresses are obtained as follows

$$\sigma_w\,(x,s) = -E\,\tilde{u}_s(s)\frac{d^2\chi}{dx^2}, \qquad (14)$$

and the corresponding warping shear flow may be deduced as

$$q_w = E\frac{d^3\chi}{dx^3}\int_0^s \tilde{u}(s)t\,ds, \qquad (15)$$

The torsional moment in each cross-section is equilibrated by the sum of uniform and non-uniform components,

$$T = T_{SV} + T_w = GJ\frac{d\phi}{dx} - EI_\omega\frac{d^3\chi}{dx^3}, \qquad (16)$$

where I_ω is a warping constant defined as

$$I_\omega = \int_S \left(\tilde{u}(s)\right)^2 t\,ds. \qquad (17)$$

On the other hand, the total shear flow and torsional moment may also be determined as

$$q = Gt\left(\frac{\partial u}{\partial s} + r\,\frac{d\phi}{dx}\right), \qquad (18)$$

$$T = \int_S q\,r\,ds = GI_c\frac{d\phi}{dx} - G\,(I_c - J)\frac{d\chi}{dx}, \qquad (19)$$

where r represents the distance from the shear centre to the wall tangent and I_c is the shear central second moment of inertia

$$I_c = \int_S r^2\,t\,ds. \qquad (20)$$

Eliminating $\frac{d\phi}{dx}$ from (16) and (19) and performing equilibrium of an infinitesimal segment of beam subjected to torsional load $m_T(x)$ leads to the differential equilibrium equation:

$$\frac{EI_\omega}{\mu}\left(\frac{d^4\chi}{dx^4}\right) + GJ\left(\frac{d^2\chi}{dx^2}\right) = m_T(x), \qquad (21)$$

where μ is the warping shear parameter given by

$$\mu = 1 - \frac{J}{I_c}. \qquad (22)$$

This parameter is a measure of the cross-sectional slenderness. For very thin walls, it approaches unity, meaning that the effect of warping shear in torsion, also designated as torsion bi-shear, has little expression.

The torsion behaviour in composite box-girders can be once again computed assuming ${t_t}^S = t_t\,G_c/G_s \approx t_t\,/n$.

The analytical solutions for these equilibrium equations may be found in Maisel & Roll (1974).

2.4. Distortion

The distortional loads, p_d, acting on a box girder are simultaneously equilibrated by two coupled mechanisms: longitudinal bending of the plates, related to loads p_d^L, and transverse deformation of the cross-section, related to loads p_d^T. The sum of the two contributions in each plate should render the total force, i.e.,

$$p_d = p_d^L + p_d^T. \qquad (23)$$

The p_d^L forces may be obtained conducting the longitudinal analysis of a segment of box girder (see Figure 3a), ensuring that the longitudinal normal stresses at the web-flange connections are continuous (see Figure 3b).

It is possible to define the longitudinal stresses in the intersections as a function of the bending moment $m_{w,d}^L$, which comes from analysing the web as a beam subjected to $p_{w,d}^L$:

$$\sigma_{2,d} = -\frac{m_{w,d}^L\,y_t}{2\,I_{w,e}}, \quad \sigma_{3,d} = \frac{m_{w,d}^L\,y_b}{2\,I_{w,e}}, \qquad (24)$$

where

$$I_{w,e} = \frac{2\beta\,[(\alpha_t+2)(\alpha_b+2)-1]}{(1+\beta)[\alpha_t+\alpha_b\beta+3(1+\beta)]}, \qquad (25)$$

$$y_t = \frac{(1+\beta)(1+\alpha_b\beta+2\beta)}{\alpha_t+\alpha_b\beta+3(1+\beta)}b_w, \qquad (26)$$

$$y_b = b_w - y_t. \qquad (27)$$

The stress diagram for the cross-section is completely defined, since it is anti-symmetrical and linear. The longitudinal equilibrium equation can be written as a function of the web in-plane displacements Δ_w:

$$p_{w,d}^L = \frac{d^4\Delta_w}{dx^4}\,EI_{w,e}. \qquad (28)$$

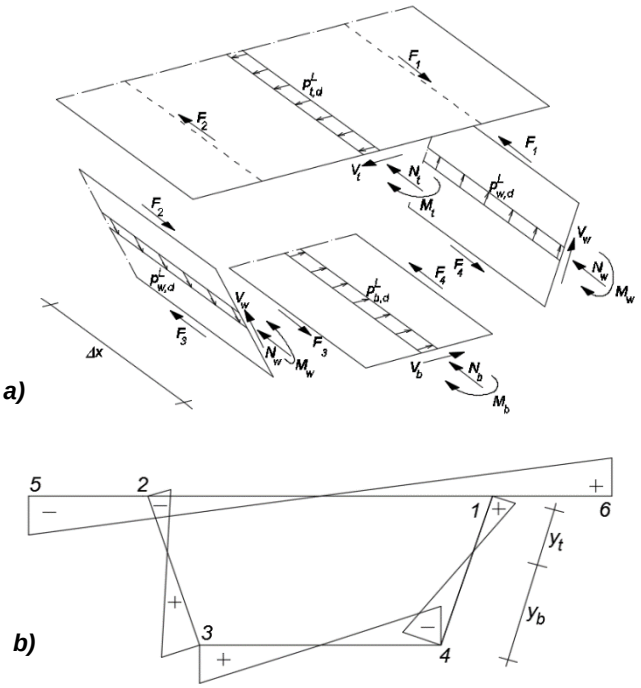

Figure 3 – a) Membrane forces and moments acting on the plates of a segment of box girder bridge subjected to distortion and b) generic distortional warping stresses

The forces p_d^T are related with the analysis of the cross-section as an individual frame. They are equivalent to anti-symmetric diagonal loads which cause transverse bending (see Figure 4).

Applying the unit dummy load method and relating the diagonal displacements with the in-plane displacements of the web plates, one can arrive at an equilibrium equation that relates $p_{w,d}^T$ and Δ_w through and equivalent "frame stiffness" k:

$$p_{w,d}^T = k\,\Delta_w, \qquad (29)$$

where

$$k = \frac{24\, b_w}{{b_b}^2 d^2} k_1 k_2 E \frac{{t_w}^3}{12(1-\nu_w)}, \qquad (30)$$

$$k_1 = \frac{[\alpha_t + \beta^2(\alpha_b + 2) + 2(\beta + 1)]\,(1+\beta)}{\alpha_t + \alpha_b \beta + 3(\beta + 1)}, \qquad (31)$$

$$k_2 = \frac{2 + 2\beta + 2\beta^2 + r_t + r_b \beta^2}{\beta[(r_t + 2)(r_b + 2) - 1]}. \qquad (32)$$

Replacing (28) and (29) into (23), one can obtain the global equilibrium equation for distortion, which is equal to (3) but with an additional term which represents the elastic foundation.

$$p_{w,d} = \frac{d^4 \Delta_w}{dx^4} EI_{w,e} + k\, \Delta_w. \qquad (33)$$

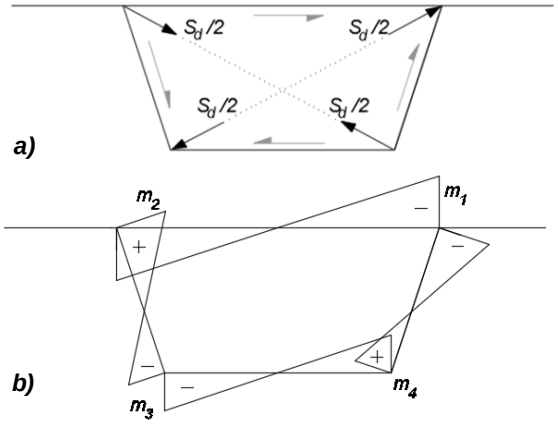

Figure 4 - a) Equivalent diagonal loads and b) corresponding transverse bending moments

The solutions to the beam on elastic foundation equation have been studied to some extent by Hetenyi (1979), and are the basis of the work by Pedro (1995), that compiled and synthetized the results for concentrated and uniformly distributed loads in both simply supported and fixed-ended spans.

When dealing with composite steel-concrete box girders, it is necessary to employ two different equivalent thicknesses. This has to do with the fact that in the longitudinal bending of the plates, the membrane bending behaviour is prominent, whereas the frame behaviour is ruled by transverse bending and hence, transverse inertias:

- Longitudinal bending (determination of $I_{w,e}$)

$$({t_t}^S)_d^L = t_t\, n = t_t \frac{E_s}{E_c}. \qquad (34)$$

- Transverse bending (determination of k)

$$({t_t}^S)_d^L = t_t \sqrt[3]{n}.$$

The longitudinal normal stresses may still be calculated employing (5).

3. Overview of Generalized Beam Theory

The longitudinal analysis of thin-walled box girder bridge decks may be performed through a finite element model based on the Generalized Beam Theory (GBT), which can capture of the effects of bending, torsion, distortion and shear lag in the longitudinal normal stresses (besides other effects). These effects shall be included through appropriate deformation modes, whose displacement shapes are pre-determined and whose amplitudes along the span are the problem unknowns.

3.1. Fundamental Formulations

For each wall of the prismatic member, this theory employs Kirchhoff's assumption for thin plates to express the displacement vector, $\boldsymbol{U}$, in terms of the wall mid-surface local axes (see Figure 5) as

$$\boldsymbol{U}(x,y,z) = \begin{bmatrix} U_x \\ U_y \\ U_z \end{bmatrix} = \begin{bmatrix} 0 & \overline{\boldsymbol{u}}^t \\ \overline{\boldsymbol{v}}^t & 0 \\ \overline{\boldsymbol{w}}^t & 0 \end{bmatrix} \begin{bmatrix} \boldsymbol{\Phi} \\ \boldsymbol{\Phi}_{,x} \end{bmatrix} - z \begin{bmatrix} 0 & \overline{\boldsymbol{w}}^t \\ {\overline{\boldsymbol{w}}_{,y}}^t & 0 \\ 0 & 0 \end{bmatrix} \begin{bmatrix} \boldsymbol{\Phi} \\ \boldsymbol{\Phi}_{,x} \end{bmatrix} = \boldsymbol{\Xi}_U \begin{bmatrix} \boldsymbol{\Phi} \\ \boldsymbol{\Phi}_{,x} \end{bmatrix}, \qquad (35)$$

where the comma indicates a differentiation, $\boldsymbol{\Phi} = \boldsymbol{\Phi}(x)$ is a column vector containing the deformation mode amplitude functions, $\boldsymbol{\Xi}_U$ is an auxiliary modal matrix and $\overline{\boldsymbol{u}}$, $\overline{\boldsymbol{v}}$ and $\overline{\boldsymbol{w}}$ are column vectors containing the deformation mode wall mid-line displacement components along the x, y and z local axes.

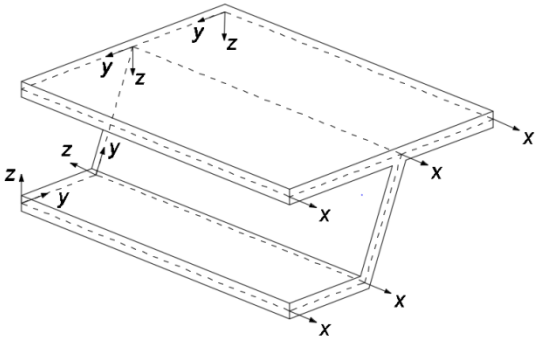

Figure 5 – Arbitrary thin-walled member geometry and local coordinate systems

Several papers have contributed to the definition of the deformation modes for arbitrary polygonal shaped cross-sections, (see for example Gonçalves, Ritto-Corrêa, & Camotim (2010), Gonçalves, Bebiano, & Camotim (2014) and Bebiano, Gonçalves, & Camotim (2015)).

The non-null components of the strain vector $\boldsymbol{\varepsilon}^t = [\, \varepsilon_{xx}\ \varepsilon_{yy}\ \varepsilon_{zz}\,]$ can be subdivided into membrane $[\,]^M$ and flexural $[\,]^F$ components:

$$\boldsymbol{\varepsilon} = \boldsymbol{\varepsilon}^M + \boldsymbol{\varepsilon}^F = (\boldsymbol{\Xi}_\varepsilon^M + z\boldsymbol{\Xi}_\varepsilon^F) \begin{bmatrix} \boldsymbol{\Phi} \\ \boldsymbol{\Phi}_{,x} \\ \boldsymbol{\Phi}_{,xx} \end{bmatrix} = \boldsymbol{\Xi}_\varepsilon \begin{bmatrix} \boldsymbol{\Phi} \\ \boldsymbol{\Phi}_{,x} \\ \boldsymbol{\Phi}_{,xx} \end{bmatrix}, \qquad (36)$$

where the auxiliary modal matrices are defined as

$$\boldsymbol{\Xi}_\varepsilon^M = \begin{bmatrix} 0 & 0 & \overline{\boldsymbol{u}}^t \\ {\overline{\boldsymbol{v}}_{,y}}^t & 0 & 0 \\ 0 & (\overline{\boldsymbol{u}}_{,y} + \boldsymbol{\nu})^t & 0 \end{bmatrix}, \qquad (37)$$

$$\boldsymbol{\Xi}_\varepsilon^F = -\begin{bmatrix} 0 & 0 & \overline{\boldsymbol{w}}^t \\ {\overline{\boldsymbol{w}}_{,yy}}^t & 0 & 0 \\ 0 & 2{\overline{\boldsymbol{w}}_{,y}}^t & 0 \end{bmatrix}. \qquad (38)$$

The stresses can be easily obtained through a constitutive relation operator $\boldsymbol{C_e}$, which in this case refers to isotropic linear elastic materials and, assuming a plane stress.

$$\begin{Bmatrix} \sigma_{xx} \\ \sigma_{yy} \\ \tau_{xy} \end{Bmatrix} = \boldsymbol{C_e} \begin{Bmatrix} \varepsilon_{xx} \\ \varepsilon_{yy} \\ \gamma_{xy} \end{Bmatrix} = \begin{bmatrix} \frac{\alpha E}{1-\nu^2} & \frac{\nu E}{1-\nu^2} & 0 \\ \frac{\nu E}{1-\nu^2} & \frac{\alpha E}{1-\nu^2} & 0 \\ 0 & 0 & G \end{bmatrix} \begin{Bmatrix} \varepsilon_{xx} \\ \varepsilon_{yy} \\ \gamma_{xy} \end{Bmatrix}. \qquad (39)$$

Here, α is a factor that equals 1 unless wall membrane transverse extensions are assumed null ($\varepsilon_{yy}^M = 0$), in which case $\alpha = (1-\nu^2)$ is adopted for the membrane terms to avoid over-stiff solutions.

The GBT equilibrium equation system is obtained from a variational principle, such as the Principle of Virtual Work (PTV). The internal work may be shown to read

$$\delta W_{int} = -\int_L \begin{bmatrix} \delta\boldsymbol{\Phi} \\ \delta\boldsymbol{\Phi}_{,x} \\ \delta\boldsymbol{\Phi}_{,xx} \end{bmatrix}^T \begin{bmatrix} \boldsymbol{B} & [\boldsymbol{0}] & \boldsymbol{D_2} \\ [\boldsymbol{0}] & \boldsymbol{D_1} & [\boldsymbol{0}] \\ \boldsymbol{D_2}^t & [\boldsymbol{0}] & \boldsymbol{C} \end{bmatrix} \begin{bmatrix} d\boldsymbol{\Phi} \\ d\boldsymbol{\Phi}_{,x} \\ d\boldsymbol{\Phi}_{,xx} \end{bmatrix} dx, \quad (40)$$

where L is the length of the member and $\boldsymbol{B}$, $\boldsymbol{C}$, $\boldsymbol{D_1}$, $\boldsymbol{D_2}$ and $\boldsymbol{D_2}^t$ are the GBT linear stiffness matrices. Each of them is associated with distinct strain components, namely transverse extension/bending, primary/secondary warping, membrane/ flexural shear and membrane/flexural Poisson effects, respectively. Assuming that the transverse extension modes shall be discarded from the analysis, these matrices are defined as

$$\begin{aligned} B_{ij} &= {B_{ij}}^F = \int_S \frac{Et^3}{12(1-\nu^2)} w_{i,yy} w_{j,yy}\, dy, \\ C_{ij} &= {C_{ij}}^M + {C_{ij}}^F = \int_S Et u_i u_j\, dy + \int_S \frac{Et^3}{12(1-\nu^2)} w_i w_j\, dy, \\ D_{1_{ij}} &= {D_{1}}_{ij}^M + {D_{1}}_{ij}^F = \int_S Gt\left(u_{i,y} + v_i\right)\left(u_{j,y} + v_j\right) dy + \\ &\quad \int_S \frac{Gt^3}{3} w_i w_j\, dy, \\ D_{2_{ij}} &= {D_{2}}_{ij}^F = \int_S \frac{\nu Et^3}{12(1-\nu^2)} w_i w_{j,yy}\, dy. \end{aligned} \quad (41)$$

Furthermore, assuming that loads are applied at the walls mid-plane, the external work can be written as

$$\delta W_{ext} = \int_\Omega \begin{bmatrix} \delta\boldsymbol{\Phi} \\ \delta\boldsymbol{\Phi}_{,x} \end{bmatrix}^t \boldsymbol{\Xi_U}^t \boldsymbol{f}\, d\Omega, \quad (42)$$

where $\boldsymbol{f}^t = [\, f_x \; f_y \; f_z \,]$ is the external load vector.

3.2. Deformation Modes

The deformation modes employed in this work can be subdivided into distinct sets (or families). The first set to be considered here (see Figure 7) consists of the so called "Vlasov's modes", i.e., the modes where Vlasov's null membrane shear strain hypothesis is employed ($\gamma_{xy}^M = 0$). It includes axial extension (mode 1), major and minor axis bending (modes 2 and 3, respectively) and distortion (mode 4).

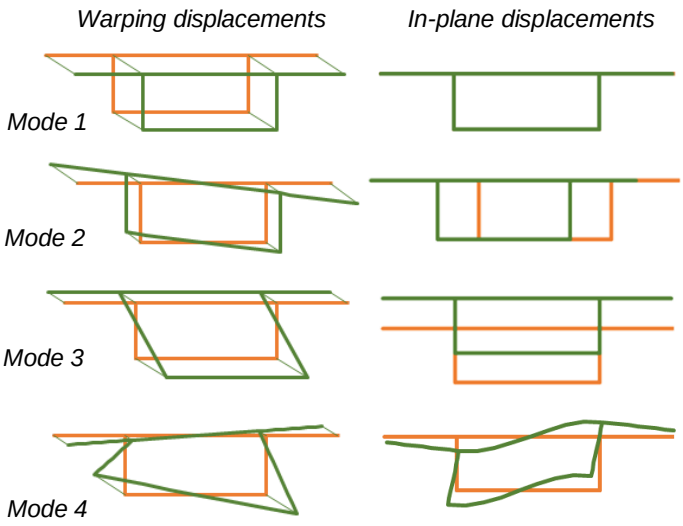

Figure 7 – Set of Vlasov's deformation modes

For comparison with the Classical Formulations, it should be pointed out that all these modes are orthogonal with respect to matrix $\boldsymbol{C}$. Furthermore, their respective in-plane displacements v and w are determined performing a frame type-analysis, in which u and v are linked through Vlasov's hypothesis.

A second set comprehends the deformation modes related with the shear deformation of the cross-section to torsion and distortion (see Figure 6). Mode 5 consists of torsion, i.e., the deformed shape of the cross-section when considering a constant shear flow circulating around the closed perimeter, being orthogonal with respect to $\boldsymbol{C}$ against modes 1 through 3 (hence it does not produce axial force nor bending, but it is not orthogonal with respect to distortion). The effect of torsion bi-shear can be replicated by taking into account an additional mode (mode 6), which has the same warping function as that associated with mode 5. Even though it is not addressed in the Classical Formulations, the effect of bi-shear in distortion may also be considered in GBT analysis by including mode 7.

The last set of deformation modes consists on further shear

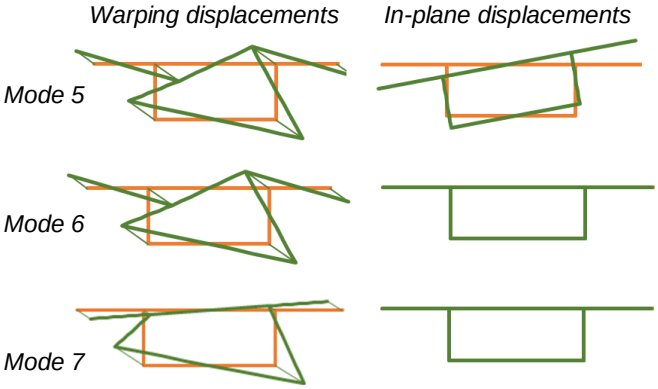

Figure 6 – Set of torsion deformation modes

modes that seek to allow for shear lag deformation (see Figure 8). It contains both symmetric (modes 8 through 11) and anti-symmetric (modes 12 through 15) warping modes ($u_k \neq 0, v_k = w_k = 0$) in both top and bottom flanges, allowing to capture more accurately the effect of shear lag deformation in each plate. Although more modes could be considered, these were found sufficient in the analysis of the numerical examples.

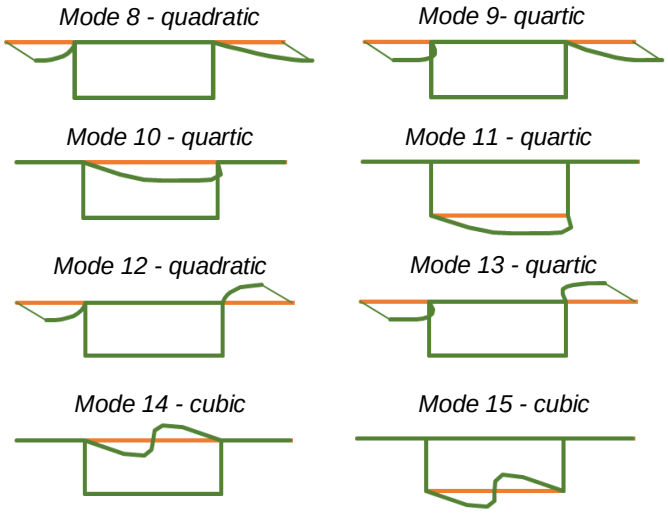

Figure 8 – Warping displacements of shear lag warping modes – Quadratic modes 8 and 12, Cubic modes 14 and 15 and Quartic modes 9,10,11 and 13 – (in-plane displacements are null).

3.3. Definition of a Finite Element and Implementation in MATLAB

In the context of longitudinal discretization, for each element, the modal amplitude functions contained in the vector $\boldsymbol{\Phi}$ can be approximated as

$$\boldsymbol{\Phi}(x) = \boldsymbol{\Psi}(x)\,\boldsymbol{d_e}, \qquad (43)$$

where $\boldsymbol{\Psi}$ is the matrix containing the longitudinal shape functions, and $\boldsymbol{d_e}$ is the vector containing the degrees of freedom of the element, which are nodal values for the amplitude functions and their derivatives.

As can be seen in (35), the displacements $\boldsymbol{U}(x,y,z)$ are a function of a first derivative with respect to the x axis, thus requiring C^1 class functions. In this situation, it is possible to make use of Hermite's cubic interpolation functions. For pure warping modes k ($\bar{u}_k \neq 0, \bar{v}_k = \bar{w}_k = 0$), these interpolation functions cannot be utilized, because the amplitude is given not as a function of Φ_k but only of $\Phi_{k,x}$ (see (35)) and that would lead to a linear dependence of H_1 and H_3. To circumvent this issue, in such situations Lagrange's linear and quadratic hierarchic polynomials are employed.

The combination of the set of these shape functions leads to a finite element with three nodes, where the first node ($x = 0$) is associated with H_1, H_2 and F_1, the second node ($x = {}^{l_i}/_{2}$) refers strictly to function F_3 and the third and final node ($x = l_i$) is related to H_3, H_4 and F_2. For a set of N deformation modes subdivided into warping (N_w) and non-warping modes, shape function matrix $\boldsymbol{\Psi}$ of dimensions $N \times (4N - N_w)$ can be organized as

$$\boldsymbol{\Psi} = \left[\begin{array}{c|c|c|c|c|c|c|c} \widetilde{\boldsymbol{H_1}} & 0 & \widetilde{\boldsymbol{H_2}} & 0 & \widetilde{\boldsymbol{H_3}} & 0 & \widetilde{\boldsymbol{H_4}} \\ 0 & P(\widetilde{\boldsymbol{F_1}}) & 0 & P(\widetilde{\boldsymbol{F_3}}) & 0 & P(\widetilde{\boldsymbol{F_2}}) & 0 \end{array}\right], \qquad (44)$$

where $\widetilde{\boldsymbol{X}}$ is a diagonal matrix sized after the number of associated deformation modes in which each term is equal to X and $P()$ is the operator for primitivation.

The element stiffness matrix $\boldsymbol{K_e}$ and the equivalent nodal force vector $\boldsymbol{F_e}$ are obtained through integrations along the element length l_i and mid-surface Ω_e as follows

$$\boldsymbol{K_e} = \int_{l_i} \begin{bmatrix} \boldsymbol{\Psi} \\ \boldsymbol{\Psi}_{,x} \\ \boldsymbol{\Psi}_{,xx} \end{bmatrix}^T \boldsymbol{M} \begin{bmatrix} \boldsymbol{\Psi} \\ \boldsymbol{\Psi}_{,x} \\ \boldsymbol{\Psi}_{,xx} \end{bmatrix} dx, \qquad (45)$$

$$\boldsymbol{F_e} = \int_{\Omega_e} \begin{bmatrix} \boldsymbol{\Psi} \\ \boldsymbol{\Psi}_{,x} \end{bmatrix}^t {\boldsymbol{\Xi}_U}^t \boldsymbol{f}\, d\Omega. \qquad (46)$$

Assembling the global stiffness matrix and force vector**,** one can determine $\boldsymbol{d}$ through the global equilibrium system of equations, and use the corresponding element nodal displacements to compute the longitudinal stresses as

$$\sigma_{xx} = \sigma_{xx}^M + \sigma_{xx}^F = E(\overline{\boldsymbol{u}}^t \boldsymbol{\Psi}_{,xx})\boldsymbol{d_e} - \frac{E}{1-\nu^2}\left(z\overline{\boldsymbol{w}}^t \boldsymbol{\Psi}_{,xx}\right)\boldsymbol{d_e} \qquad (47)$$

The transverse discretization is useful only for the determination of the deformation modes. The displacements of modes 1 through 5 are obtained through numerical program GBTUL (available at http://www.civil.ist.utl.pt/gbt/), in which the box girder is subdivided into six walls, connected at their intersections. Modes 6 and 7 are defined by the warping displacements of modes 5 and 4, respectively, and the additional shear lag modes can be defined analytically.

The routine developed in MATLAB allows for the orthogonalization of the shear lag modes 8 through 15 with respect to matrix $\boldsymbol{C}$. This will result in the uncoupling of each mode's participation in the total longitudinal normal stresses.

4. Theoretical Comparison between Classical Formulations and Generalized Beam Theory

It is possible to put into evidence some of the theoretical differences between the two approaches detailed so far. Both consider several cross-section deformation modes, which are variable along the longitudinal axis of the member. For each approach, the modes' amplitude functions can be determined by means of equilibrium equations. Thus, the comparison between the two becomes more clear when analysing separately each method's (i) pre-defined deformation modes and (ii) established longitudinal equilibrium equations.

4.1. Comparison of the Cross-section Deformation Modes

Each cross-section deformation mode k is simultaneously characterized by its in-plane (v_k, w_k) and out-of-plane displacements (u_k). For the case of minor-axis bending, both approaches assume an in-plane rigid body translation of the cross-section, which remains normal to the longitudinal axis.

When dealing with non-uniform torsion accounting for the effect of bi-shear, the Classical Formulations consider that the warping displacements do not depend only on the in-plane rigid body behaviour, i.e., two distinct deformation modes are considered, one concerning the rigid body rotation ($\phi(x)$) and another related to the warping displacements of the cross-section ($\chi(x)$). The deformation field is obtained by the linear combination of these two modes. Since the "shape" of the GBT warping displacements matches the one in the Classical Formulations ($\widetilde{u_S}(s)$), the deformation field obtained by their linear combination is necessarily the same mode space.

The definition of the distortional deformation mode in the Classical Formulations is based on the combination of the longitudinal bending behaviour of the plates with a transverse frame-type response. In the longitudinal analysis, Vlasov's hypothesis is implicitly assumed. In the frame analysis, transverse extension of the walls is neglected, meaning once again that the classical definition of the distortional deformed configuration coincides with the one presented in GBT.

As far as shear lag effects are concerned, the Classical Formulations make use of a single global shear lag mode, whereas GBT analyses allow for the consideration of a broad set of modes. Evidently, this should result in higher accuracy when using the GBT-based approach, because the effect of shear lag deformability may vary along the plates in a rather complex way. Even so, it should be pointed out that the most of the GBT shear lag modes were defined as quartic based on the classical expressions for shear lag in bending.

Finally, it should be noted that GBT does not require homogenization and therefore, for composite cross-sections, the homogenisation procedures employed in the Classical Formulations may lead to slight differences.

4.2. Comparison of the Longitudinal Equilibrium Equations

The GBT equilibrium equations can be written in the differential form as

$$\boldsymbol{C\Phi}_{,xxxx} - \left(\boldsymbol{D_1} - \boldsymbol{D_2} - {\boldsymbol{D_2}}^t\right)\boldsymbol{\Phi}_{,xx} + \boldsymbol{B\Phi} = \boldsymbol{f}_{x,x} + \boldsymbol{f}_y + \boldsymbol{f}_z \qquad (48)$$

As for the Classical Formulations, the equivalent expressions for bending, torsion with warping and distortion can be obtained from those in (3), (16), (19) and (33) and expressed in matrix form so that

$$\begin{bmatrix} EI_y & 0 & 0 & 0 \\ 0 & EI_\omega & 0 & 0 \\ 0 & 0 & 0 & 0 \\ 0 & 0 & 0 & -EI_{w,e}\dfrac{p\cos\varphi}{p_{w,d}} \end{bmatrix} \begin{bmatrix} v_{,xxxx} \\ \chi_{,xxxx} \\ \phi_{,xxxx} \\ \Delta_{w,xxxx} \end{bmatrix} + \begin{bmatrix} 0 & 0 & 0 & 0 \\ 0 & -G(J-I_c) & G(J-I_c) & 0 \\ 0 & G(J-I_c) & GI_c & 0 \\ 0 & 0 & 0 & 0 \end{bmatrix} \begin{bmatrix} v_{,xx} \\ \chi_{,xx} \\ \phi_{,xx} \\ \Delta_{w,xx} \end{bmatrix} + \begin{bmatrix} 0 & 0 & 0 & 0 \\ 0 & 0 & 0 & 0 \\ 0 & 0 & 0 & 0 \\ 0 & 0 & 0 & k\dfrac{p\cos\varphi}{p_{w,d}} \end{bmatrix} \begin{bmatrix} v \\ \chi \\ \phi \\ \Delta_x \end{bmatrix} = \begin{bmatrix} p \\ 0 \\ m \\ p \end{bmatrix} \quad (49)$$

It is possible to notice that the amplitude functions Φ_k are respectively given in terms of the vertical displacement of the cross-section v, of the warping function χ, of the angle of twist ϕ and of the in-plane displacement of the web Δ_w.

Through the GBT approach, the equivalent system comes

$$\begin{bmatrix} C_{vv} & 0 & 0 & 0 \\ 0 & {C_{\chi\chi}}^M & 0 & {C_{\Delta_w\chi}}^M \\ 0 & 0 & {C_{\phi\phi}}^F & {C_{\Delta_w\phi}}^F \\ 0 & {C_{\chi\Delta_w}}^M & {C_{\phi\Delta_w}}^F & {C_{\Delta_w\Delta_w}}^F \end{bmatrix} \begin{bmatrix} v_{,xxxx} \\ \chi_{,xxxx} \\ \phi_{,xxxx} \\ \Delta_{w,xxxx} \end{bmatrix} + \begin{bmatrix} 0 & 0 & 0 & 0 \\ 0 & {D_{\chi\chi}}^M & {D_{\phi\chi}}^M & 0 \\ 0 & {D_{\chi\phi}}^M & D_{\phi\phi} & {D_{\Delta_w\phi}}^F \\ 0 & 0 & {D_{\phi\Delta_w}}^F & {D_{\Delta_w\Delta_w}}^F \end{bmatrix} \begin{bmatrix} v_{,xx} \\ \chi_{,xx} \\ \phi_{,xx} \\ \Delta_{w,xx} \end{bmatrix} + \begin{bmatrix} 0 & 0 & 0 & 0 \\ 0 & 0 & 0 & 0 \\ 0 & 0 & 0 & 0 \\ 0 & 0 & 0 & {B_{\Delta_w\Delta_w}}^F \end{bmatrix} \begin{bmatrix} v \\ \chi \\ \phi \\ \Delta_x \end{bmatrix} = \begin{bmatrix} p \\ 0 \\ m \\ p \end{bmatrix} \quad (50)$$

At this point, it can be concluded that the GBT torsion and distortion equations are coupled, as seen by the existence of non-diagonal terms in the last three lines of the system of equations. In the Classical Formulations these terms are null, because (i) several of these coefficients relate to wall flexural behaviour, which is often disregarded in more classical approaches and (ii) in the determination of $p_{w,d}$ the effect of torsion bi-shear deformation was neglected.

In terms of the solutions to these equations, since Kirchhoff's hypothesis was adopted, in GBT formulation the longitudinal amplitude functions are always at least of class C^1. The same is not always true in Classical Formulations, where in some cases, such as in the torsional response case, it suffices that the displacements be C^0 continuous. This will lead to additional discrepancies in the results for sections near concentrated loads, diaphragms and supports.

In conclusion, even though the cross-section deformation modes generally coincide, the Classical Formulations present differences with respect to the GBT, which originate differences in the longitudinal stress distributions. Recall that shear lag has not been considered in this section.

5. Analysis of Numerical Examples

5.1. Numerical Example 1

This first example deals with a simply supported 30 m span concrete box-girder deck of constant cross-section acted by a mid-span concentrated load Q, and a uniform longitudinal line load q, both applied in one of the web-top slab joints (see Figure 9a). Diaphragms exist at the support sections only.

The mid-surface longitudinal stresses which are here subject of comparison were obtained through (i) the Classical Formulations (ii) a GBT displacement-based finite element model using 30 elements of equal length and (iii) a shell finite element model using 1800 4-node shell elements in the commercial program ADINA. Figure 9b presents the cross-section σ_{xx}^M diagrams for the mid-span section and the longitudinal σ_{xx}^M diagram for the loaded web-top flange intersection line, and Figure 9c shows the modal participations for both methods, with respect to the concentrated load.

The GBT results show very good agreement with those obtained with the shell finite element model. The stresses obtained following the Classical Formulations appear to be a good estimate but deviate more with respect to the FEM stress curves, especially for the mid-span concentrated load case.

It is possible to observe that, in general, the Classical Formulations have modal participations similar to those obtained in the GBT analysis. Higher discrepancies are noticed in terms of the shear lag effects. The results for bending coincide and those for torsion with warping including bi-shear are very similar. The same does not happen however for the distortional mode, in which the GBT formulation generally leads to smaller stresses throughout the span. This happens due to the reasons explained in section 4, as well as due to the inclusion of distortion bi-shear in the GBT approach.

5.2. Numerical Example 2

The second case study is a simply supported composite steel-concrete box-girder bridge subjected to self-weight and to Load Model 1 traffic actions defined in NP EN 1991-2. The thickness of both steel and concrete walls is constant along a 36-meter span (see Figure 9d). Three different situations are considered in what regards the diaphragm spacing: every 7.2 meters, every 12 meters and every 36 meters (corresponds to having diaphragms at the end supports only).

In what regards global verifications, NP EN 1991-2 states that the uniformly distributed loads should be applied only in the unfavourable part of the influence surface, both longitudinally and transversally. Naturally, considering that the entire area of the notional lane is loaded will lead to the maximum longitudinal bending stresses. However, such would produce null longitudinal stresses from torsion and distortion, since the so-called notional lane is centred with the axis of symmetry.

For this reason, one should also take into consideration load cases 2 and 3 (see Figure 9e), in an attempt to maximize torsion and distortion effects, because those situations might be more unfavourable. The sum of torsional and distortional stresses due to the two load cases and in the two situations with intermediate diaphragms are presented in Figures 9f.

First, comparing the values of these stresses with the number of span diaphragms, it is clear the important effect in reducing the longitudinal stresses due to torsion presented by this transversal restrain of the cross-section deformation.

Secondly, although not shown here, the influence of torsion is negligible, except for sections in the vicinities of the diaphragm. Hence, the overall behaviour is governed by the distortional response, which is similar to that of a continuous beam on an elastic foundation. For this reason, it is possible to approximate the mid-span stresses through equivalent fixed-ended (load case 3) and simply supported (load case 2) spans with a length equal to the spacing between diaphragms.

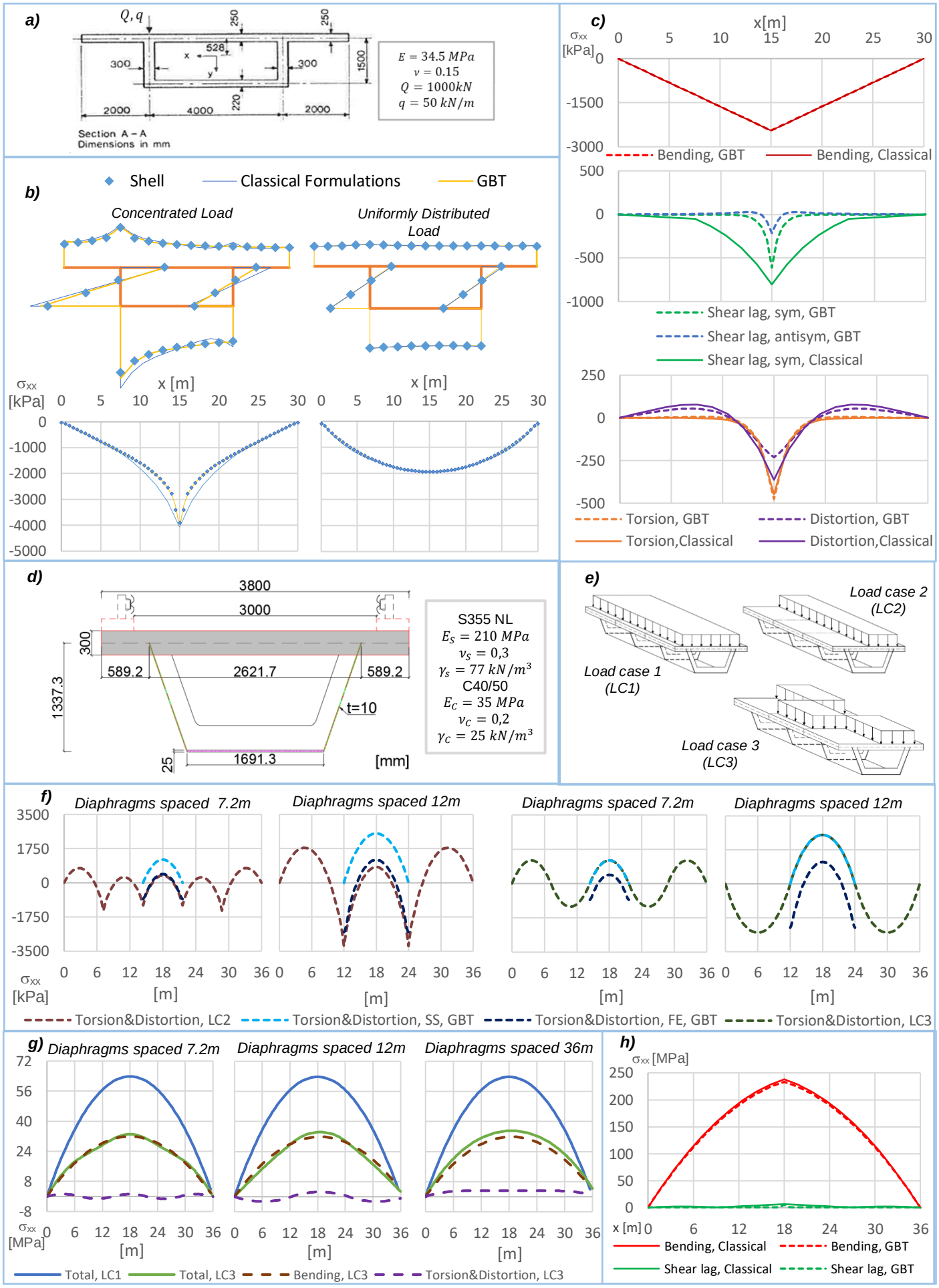

Figure 9 – a) Geometry and other parameters for NE1 (numerical example 1); b) cross-section and longitudinal stress profiles for NE1; c) modal stress participations for concentrated load in NE1; d) Geometry and other parameters for NE2; e) Load cases (LC) in NE2; f) Longitudinal profiles of added torsion and distortion stresses for LC2 and LC3 and comparison with equivalent simply supported (SS) and fixed-ended (FE) spans; g) Comparison between maximum I stresses of LC1 and LC3; h) Modal participations to the maximum stresses for characteristic combination in NE2

These results provide some guidance concerning the application of the Classical Formulations for box girders with intermediate spans. Although not shown, considering the same equivalent spans and boundary conditions did not lead to equally satisfactory results, but seemed to offer an upper bound for the longitudinal stresses at mid-span.

Readdressing the subject of the global analysis of the box-girder bridge subjected to uniform loads, it can be observed that load case 3 provides mid-span longitudinal stress which are substantially higher than the ones obtained for load case 2. There is an increase in about 216% and 212% for the configurations with 4 and 2 intermediate diaphragms, respectively. Even so, for this example, load case 1 continues to govern design for all diaphragm spacing configurations (see Figure 9g) and must be considered for the determination of the total stresses for the characteristic combination, which depend solely on bending and shear lag (see Figure 9h).

6. Conclusions

The present works revolves around the longitudinal analysis of mainly steel-concrete composite box girder decks, through the use of two distinct methods of analysis that allow for a strong perception of the structural behaviour: one concerning the so-called Classical Formulations and another based on the Generalized Beam Theory.

The main conclusions of this work are:

1. The definition of the cross-section deformation modes in the both approaches, is equivalent in terms of the membrane displacements of bending, torsion with warping and distortion. Some minor differences may occur in composite steel-concrete cross-sections due to the simplifications pertaining to the homogenization rules used in the Classical Formulations.
2. The shear lag effect in the Classical Formulations is semi-empirical and entails a single global symmetric shear lag mode. GBT allows capturing shear lag through more modes, namely symmetric and anti-symmetric modes.
3. The GBT approach allows obtaining equations which are similar to the ones of the Classical Formulations, but more complex because they consider (i) several wall flexural contributions that are neglected in the latter and (ii) the coupling of bi-shear and distortion.
4. For the Classical Formulations, the shear lag effect in numerical example 1 does not show a good agreement with the stresses obtained with a shell finite element model, both in terms of longitudinal and cross-section diagrams. With the GBT approach it was possible to obtain results that agree very well with the shell FEM results. For this outcome, the presence of anti-symmetric shear lag modes was found to be relevant. For the numerical example 2, the shear lag effects are not as meaningful because the flanges are narrow.
5. The results of torsion with warping are similar but do not coincide. For distortion, longitudinal stress results are further apart, due to the additional simplifications considered in the Classical Formulations, namely the non-inclusion of distortion bi-shear.
6. The added torsional and distortional longitudinal stress profiles (including bi-shear) are similar to those obtained conducting the analysis of a continuous beam on an elastic foundation, when intermediate diaphragms are considered.
7. Three different load cases for the uniform loading in numerical example 2 were considered, covering the most unfavourable design situations: (i) roadway fully loaded, (ii) roadway is loaded only on one side of the plane of symmetry and (iii) roadway between each diaphragm is loaded only on one side of the plane of symmetry, but with the side alternating after each diaphragm span. The stresses obtained considering the third load case were much higher than those obtained in the second.
8. In overall, the Classical Formulations resort to more simplifications than GBT and this affects the accuracy of the results, although generally on the safe side.
9. The consideration of the shear lag effect in GBT is fairly simple. GBT is also more versatile and naturally more accurate than the use of effective width coefficients.
10. The Classical Formulations comprise a fast and insightful tool, very valuable to obtain a first estimate of the longitudinal stresses due to bending with shear lag, torsion with warping and distortion.
11. The Generalized Beam Theory approach shows a great potential as a design tool, because it allows analysing the modal participation and thus extract conclusions concerning the structural behaviour, while being based on a simple and broad formulation that can produce very accurate results.

References

B.S.I. BS 5400 - Steel, concrete and composite bridges. Code of practice for design of composite bridges - Part 3: Code of practice for design of steel bridges (2004).

Bebiano, R., Gonçalves, R., & Camotim, D. (2015). A cross-section analysis procedure to rationalise and automate the performance of GBT-based structural analyses. *Thin-Walled Structures*, *92*, 29–47.

Benscoter, S. U. (1954). A theory of torsion bending for multicell beams. *Journal of Applied Mechanics*, *21*(1), 25–34.

Castro, J. M., Elghazouli, A. Y., & Izzuddin, B. A. (2007). Assessment of effective slab widths in composite beams. *J. Constructional Steel Research*, *63*(10), 1317–27

Chen, Y. S., & Yen, B. T. (1980). *Analysis of Composite Box Girders* Fritz Laboratory Reports, Nº380-12.

Fan, Z. T., & Helwig, T. A (2002). Distortional Loads and Brace Forces in Steel Box Girders. *Journal of Structural Engineering*, *128*(6), 710–718.

Gonçalves, R., Bebiano, R., & Camotim, D. (2014). On the Shear Deformation Modes in the Framework of Generalised Beam Theory. *Thin-Walled Structures*, *84*, 325–334.

Gonçalves, R., & Camotim, D. (2010). Steel-concrete composite bridge analysis using Generalised Beam Theory. *Steel and Composite Structures*, *10*(3), 223–243.

Gonçalves, R., Ritto-Corrêa, M., & Camotim, D. (2010). A new approach to the calculation of cross-section deformation modes in the framework of generalized beam theory. *Computational Mechanics*, *46*(5), 759–781.

Hetenyi, M. (1979). *Beams on elastic foundation: Theory with applications in the fields of civil and mechanical engineering* (11th ed.). The University of Michigan Press.

Kollbrunner, C., & F. Basler, K. (1969). *Torsion in Structures*. Berlin/Heidelberg: Springer-Verlag.

Maisel, B. I., & Roll, F. (1974). *Methods of analysis and design of concrete box beams with side cantilevers*. Cement and Concrete Association. London. (No. 42.494 Tech Rpt.).

Pedro, J. J. O. (1995). *Distorção em tabuleiros de pontes em caixão. Influência no comportamento longitudinal*.MSc Thesis, UTL.

Schlaich, J., & Scheef, H. (1982). *Concrete Box-Girder Bridges*. Vol.1 IABSE.

Wright, R. N., Abdel-Samed, S. R., & Robinson, A. R. (1968). BEF Analogy for Analysis of Box Girders. *Journal of the Structural Division*.